Identifying the domain-wall spin structure in antiferromagnetic NiO/Pt

C. Schmitt,[1,*] L. Sanchez-Tejerina,[2,†] M. Filianina,[1,3,‡] F. Fuhrmann,[1] H. Meer,[1] R. Ramos,[4,§] F. Maccherozzi,[5] D. Backes,[5] E. Saitoh,[4,6,7,8,9] G. Finocchio,[2] L. Baldrati,[1] and M. Kläui[1,3,‖]

[1]*Institute of Physics, Johannes Gutenberg University Mainz, 55099 Mainz, Germany*

[2]*Department of Mathematical and Computer Sciences, Physical Sciences, and Earth Sciences, University of Messina, 98166 Messina, Italy*

[3]*Graduate School of Excellence Materials Science in Mainz, 55128 Mainz, Germany*

[4]*WPI-Advanced Institute for Materials Research, Tohoku University, Sendai 980-8577, Japan*

[5]*Diamond Light Source, Harwell Science and Innovation Campus, Didcot OX11 0DE, United Kingdom*

[6]*Institute for Materials Research, Tohoku University, Sendai 980-8577, Japan*

[7]*Institute of AI and Beyond, University of Tokyo, Tokyo 113-8656, Japan*

[8]*Center for Spintronics Research Network, Tohoku University, Sendai 980-8577, Japan*

[9]*Department of Applied Physics, University of Tokyo, Tokyo 113-8656, Japan*

(Received 27 September 2022; revised 19 December 2022; accepted 6 April 2023; published 9 May 2023)

The understanding of antiferromagnetic domain walls, which are the interface between domains with different Néel order orientations, is a crucial aspect to enable the use of antiferromagnetic materials as active elements in future spintronic devices. In this work, we demonstrate that in antiferromagnetic NiO/Pt bilayers arbitrary-shaped structures can be generated by switching driven by electrical current pulses. The generated domains are T domains, separated from each other by a domain wall whose spins are pointing toward the average direction of the two T domains rather than the common axis of the two planes. Interestingly, this direction is the same for the whole domain wall indicating the absence of strong Lifshitz invariants. The domain wall can be micromagnetically modeled by strain distributions in the NiO thin film induced by the MgO substrate, deviating from the bulk anisotropy. From our measurements we determine the domain-wall width to have a full width at half maximum of $\Delta = 98 \pm 10$ nm, demonstrating strong confinement.

DOI: 10.1103/PhysRevB.107.184417

I. INTRODUCTION

Spintronic devices to date mostly rely on ferromagnets (FMs) as active elements to store magnetic information. However, antiferromagnets (AFMs) possess several advantages over FMs for use in applications such as spin dynamics in the THz regime, high stability in the presence of external magnetic fields, and a lack of magnetic stray fields. Therefore, AFMs are prime candidates to replace FMs as active elements in future spintronic devices [1,2]. In particular insulating antiferromagnetic materials are promising candidates for the development of low-power devices, because their low damping allows for the transport of pure spin currents over long distances [3].

However, a key requirement in view of applications is efficient and reliable reading and writing of magnetic information encoded in the orientation of the antiferromagnetic Néel order **n**. It has been established that electrical current pulses through an adjacent heavy-metal layer can induce a reorientation of the antiferromagnetic order in insulating AFMs [4–6]. However, the switching mechanism is highly debated [4–8]: On the one hand, for insulating AFMs with strong magnetostriction, such as NiO [9], the writing of the Néel vector is reported to be dominated by a thermomagnetoelastic switching mechanism [7,8,10] and especially for high current densities electromigration effects in the heavy-metal layer were observed [11]. On the other hand, switching mechanisms based on spin-current-induced domain-wall motion are also theoretically predicted for this class of materials [12–14] and switching experiments with current densities smaller than the ones necessary for electromigration were performed [15].

The domain walls (DWs) in antiferromagnets provide a key to understanding the magnetic microstructure [16] and the spin structure influences the thermal stability [17], magnetoresistance [18,19], and exchange bias when coupled to a FM [20] in the AFMs. Furthermore, the type of DW, Bloch or Néel or a mixture of both [21], affects their response to current-induced spin torques [6,12,13,22,23] and is also crucial to understand the magnon coupling in AFMs [24,25].

While DWs in FMs are extensively studied [16], the structure of DWs in AFMs is often unknown. Although the domains have been imaged for various materials [26–31], these studies often do not include the internal DW spin

*Christin.Schmitt@Uni-Mainz.de

†Present address: Department of Electricity and Electronics, University of Valladolid, Valladolid 47002, Spain.

‡Present address: Department of Physics, AlbaNova University Center, Stockholm University, S-106 91 Stockholm, Sweden.

§Present address: Centro Singular de Investigación en Química Biolóxica e Materiais Moleculares (CIQUS), Departamento de Química-Física, Universidade de Santiago de Compostela, Santiago de Compostela 15782, Spain.

‖Klaeui@Uni-Mainz.de

structure. The lack of experimental results is partially due to an insufficient spatial resolution of many techniques. Yet, only a few studies investigate antiferromagnetic domain walls, for example in synthetic antiferromagnets [32], monolayer thin films [33], bulk systems of Cr_2O_3 [19] and NiO [34–36], and thin films of CuMnAs [37]. Theoretically it has been predicted that DWs in thin antiferromagnetic films can become chiral due to Lifshitz invariants [38]. Due to the lack of experimental results on antiferromagnetic DWs, this has not been checked experimentally for the predicted systems, such as NiO. However, the internal domain-wall structure affects the response of antiferromagnets to excitations and governs the dynamics. This is of critical importance when considering how to read, transfer, and write magnetic information in AFMs, and thus revealing the AFM DW spin structure is a key open question.

An important material in the context of AFM spintronics is NiO, for which in thin film form the domain-wall structure is not known. NiO is considered a promising material for active elements in spintronic applications, due to the possibility of electrical control and readout of the AFM order [4,14,39,40] and observation of ultrafast currents in the THz regime in NiO/Pt bilayers [2,41]. Bulk NiO shows a simple cubic crystallographic structure above the Néel temperature of $T_N = 523$ K [42] but it contracts along the ⟨111⟩ directions below T_N. As a consequence the spins are confined into one of the four equivalent ferromagnetic {111} planes, which are coupled antiferromagnetically (T domains). Within each of these T domains, there are three easy axes along the ⟨112⟩ directions (S domains) leading to 12 possible domain orientations in bulk NiO [35,43,44]. Therefore, we can distinguish between S-domain walls, where the spin rotates but the crystallographic structure is kept, and T-domain walls, in which the direction of the distortion of the original cube changes from one [111] diagonal to another [42]. In the case of T domains, the distortion of the two adjacent domains must match, imposing certain restrictions [35]. Therefore, T-domain walls follow particular crystallographic directions. For thin films of NiO on MgO a compressive strain is induced due to the lattice mismatch. This leads to a stabilization of only the S domain with the largest out-of-plane component in each T domain, due to the strain in the out-of-plane direction [45]. Further, the Néel vector orientation is canted out-of-plane compared to the [112] direction in bulk NiO. In our thin NiO films we can distinguish four types of T domains with the Néel vector oriented along [±5 ± 5 19] [45]. Since the present domains are T domains and crystallographic restrictions are expected, an understanding of the antiferromagnetic DW configuration in NiO thin films and determining the DW chirality is of importance when considering how NiO can be used as an active element in spintronic devices.

In this work, we determine the Néel vector orientation by photoemission electron microscopy (PEEM) exploiting the x-ray magnetic linear dichroism (XMLD) effect [45] in antiferromagnetic NiO thin films grown epitaxially on MgO(001). Our results demonstrate the possibility to create domains with arbitrary shapes, for instance almost-circular-shaped antiferromagnetic domains by current-induced switching which, therefore, do not comply with the aforementioned crystallographic restrictions for the bulk case. We show by micromagnetic simulations that the nonchiral antiferromagnetic

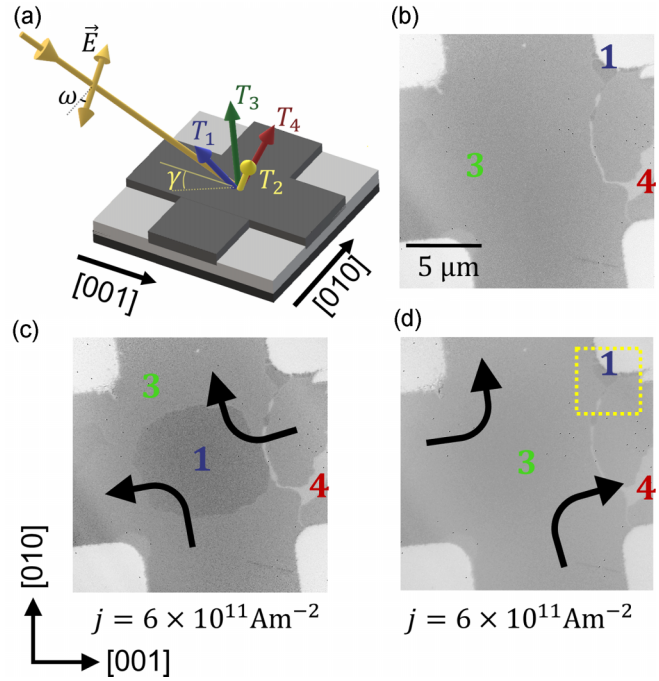

FIG. 1. (a) Experimental layout and pulsing scheme. The angles defining the linear polarization vector and the Néel vector are defined with respect to the crystallographic axes. (b) The initial state of the sample before an electric pulse was applied. (c) An approximately circular-shaped domain after the application of an X-shaped pulse along the direction indicated by the arrows. (d) After applying an X-shaped pulse with equal current density along the perpendicular direction, the circular-shaped domain vanishes and the initial state is restored. The yellow square indicates the area that is magnified in Fig. 2.

domains that we see in our samples can be explained by an anisotropy originating from the strain distribution present in the thin films. This anisotropy also agrees with the XMLD images for the DW configuration for which the Néel vector points out of the plane and we quantify the DW width to a full width at half maximum (FWHM) of $\Delta = 98 \pm 10$ nm, indicating narrow domain walls and the importance of anisotropy in our thin films.

II. RESULTS

To investigate the DW structure and the effect of electrical current pulses on this structure, we have fabricated epitaxial NiO(10 nm)/Pt(2 nm) bilayers on MgO(001) substrates, using the protocol described in Ref. [45] where we verified the antiferromagnetic ordering by the observation of x-ray magnetic linear dichroism (XMLD) and negligible x-ray magnetic circular dichroism (XMCD). In order to be able to apply electrical current pulses, a 10 µm wide Hall cross device is patterned using Ar ion beam etching. Figure 1(a) shows the device layout. The Hall cross is oriented along the [100] crystallographic axis. The four arrows represent the four T domains with the Néel vector along the [±5 ± 5 19] directions that can be present in our NiO thin films. This domain configuration allows for DWs between domains with in-plane Néel vector components differing by 90° and a DW

between two T domains with an in-plane Néel vector component with 180° difference. To acquire the XMLD-PEEM images, the Ni L_2 edge is used and the contrast is calculated as XMLD $= \frac{I(E_{\text{low}})-I(E_{\text{high}})}{I(E_{\text{low}})+I(E_{\text{high}})}$, where $E_{\text{low}} = 869.7$ eV and $E_{\text{high}} = 871.0$ eV. To electrically manipulate the Néel vector orientation, current pulses of 1 ms duration are applied to the sample. The initial state is largely single domain as Fig. 1(b) shows, in line with the reports of large domains for high-quality bulk NiO [44], and is set by the application of a pulse with a current density $j = 8.0 \times 10^{11}$ A/m^2 along the [010] direction. Only at the patterning edge of the Hall cross small domains are nucleated due to changes of the surface anisotropy at the edge due to the patterning [46]. With an X-shaped pulse (represented by the black arrows in Fig. 1(c)) with the current direction in the center of the cross along [$\bar{1}$10] and a current density of $j = 1.25 \times 10^{12}$ A/m^2 electrical switching in the center of the Hall cross is achieved and an approximately circular-shaped domain is nucleated. An X-shaped pulse [Fig. 1(d)] with equal current density but perpendicular direction along [110] (in the center of the cross) switches the magnetic order back to the initial state, as seen in Fig. 1(d).

Figure 2 shows a rotated magnification of the domains that are nucleated at the top right corner of the XMLD-PEEM image in Fig. 1(d) (indicated by a yellow frame). These magnetic structures show the same contrast and behavior as the arbitrary-shaped current-induced domains in the center of the Hall cross device, such as the approximately circular domain in Fig. 1(c). We have chosen the presented PEEM images as they have been taken with a smaller field of view and better resolution. So we will in the following concentrate on these domain structures and domain walls that are imaged with high resolution. However, the results can be transferred to the approximately circular domain and its domain wall in the center of the Hall cross showing consistent behavior for the whole sample (see Supplemental Material S1 [47]). Figure 2 shows three different types of domains nucleated at the edge of the Hall cross for different azimuthal angles γ (27°, 0°, −45°, −90°) and three different beam polarizations ω [0° (LH), 90° (LV), and a linear arbitrary angle (LA)]. One sees that when changing γ or ω the gray-scale contrast between the three domain types varies along with the projection of the x-ray polarization vector **E** on the Néel vector **n**. The way the XMLD-PEEM signal is calculated leads to the maximum XMLD signal (area with the Néel vector having the largest projection on the **E** vector) being represented in white and low-XMLD signals (area with the smallest projection of the Néel vector on the **E** vector) in black. For certain angles, e.g., $\gamma = 0°$, $\omega = 0°$, the XMLD-PEEM signal for two or for all three of the observed domains is equal, meaning that the projection of the different Néel vectors on the x-ray polarization is the same. In this case, the DW in between the domains becomes easily visible [see, e.g., Fig. 2(d)]. We can see that the XMLD-PEEM resolution is not good enough to resolve the details of the gradual rotation of the Néel vector. However, from the contrast, we can unambiguously determine the sense of rotation and from a fit of the profile we can extract the domain-wall width.

Taking into account the data for different γ and ω values, the gray-scale contrast between the individual domains

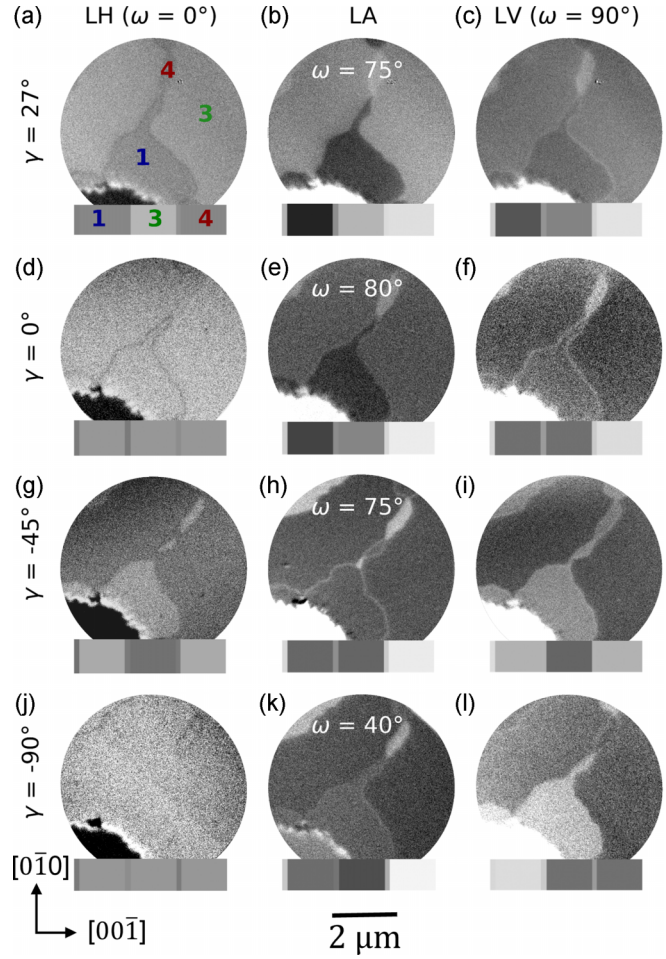

FIG. 2. Three-level domain contrast and corresponding gray-scale simulation for different azimuthal angles γ and angles of the beam polarization ω. The DW between two neighboring domains can be seen easily whenever the gray scale of the two domains is similar. The simulated gray-scale contrast considering a Néel vector angle with respect to the out-of-plane direction of $\theta = 78.7° \pm 0.3°$ is depicted below the XMLD-PEEM image. The simulated contrast matches the domain and domain-wall contrast for all combinations of azimuthal angle γ and beam polarization ω.

and domain walls, and angles where the contrast disappears and contrast inversion points, one can by visual inspection obtain information on the rotation direction of the DW. The best agreement between experimental data and contrast simulation is obtained for a canting of the Néel vector of $\theta = 78.7° \pm 0.3°$ out of the sample plane, corresponding to the [±10 ± 10 71] direction. For angles outside the error range, the x-ray polarization angle for which a contrast inversion would be expected no longer agrees with the experimental result for at least one of the azimuthal angles studied (see Supplemental Material S2 [47]). Figure 2 shows that for the determined angle of $\theta = 78.7° \pm 0.3°$, the contrast between domains and domain walls agrees with the simulated contrast for all combinations of azimuthal angles γ and polarizations ω. This indicates a rotation of the Néel vector out of the sample plane in comparison to the [±5 ± 5 19] orientation of the Néel vector in the magnetic domains [45]. From previous

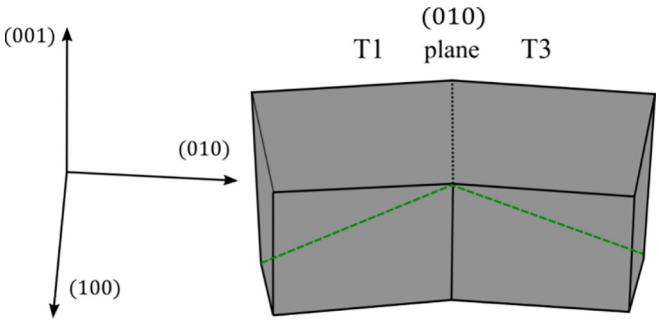

FIG. 3. An exaggerated model of the rhombohedral distortion in NiO below the Néel temperature. The green lines along the [111] diagonal and [1$\bar{1}$1] diagonal indicate the axes along which the T_1 and T_3 domain are contracted, respectively. The two domains can match sharing the (010) plane, forming a twin wall.

studies on bulk NiO one would expect a rotation of the Néel vector in a way that it crosses the diagonal shared by the two T domains since in the planes the anisotropy energy density is smallest [34]. Thus, one could expect the Néel vector to rotate in the {111} planes diminishing the anisotropy energy density [25]. This, however, would lead to a decreased out-of-plane component of the Néel vector n_z within the DW, contrary to the observation here in NiO thin films. The observed increase of the z component in Fig. 2 indicates a rotation of **n** along the shortest path from one domain to the other, even though this requires a rotation farther away from the {111} planes, which increases the anisotropy energy density. However, micromagnetic simulations suggest that this configuration, with the rotation of **n** on the shortest path between the domains, reduces the exchange energy density and the DW width, thus minimizing the total energy. We want to point out that along the entire structures, the DWs show the same contrast, meaning the orientation of the spins in the DWs is the same everywhere in the DW. Therefore, we find that in contrast to predictions [38] the DW in our NiO/Pt thin film heterostructure is not chiral.

In bulk NiO materials the crystallographic cell is contracted along one of the four possible ⟨111⟩ directions [42]. The contraction direction therefore determines different crystallographic domains, the so-called T domains. For each T domain, the spin axes are oriented in the plane perpendicular to the distortion axis; i.e., the distortion direction constitutes the hard axis, which differs for each T domain. The spin orientation in each easy plane can be described by the anisotropy energy density given in the Supplemental Material S3 [47]. However, these four possible contraction directions yield a crystallographic constraint for the DW orientation between T domains. Figure 3 shows schematically a T_1 domain, represented by a cube slightly contracted along the [111] diagonal (indicated by the green line), and a T_3 domain, represented by a cube slightly contracted along the [1$\bar{1}$1] diagonal. These two types of domains can match sharing the (010) plane, forming a twin wall. If the cube is contracted along another [111] diagonal, the two domains cannot share that plane. It follows then that two T domains cannot form arbitrary-shaped domains in bulk materials. To understand the rotation of the Néel vector within the DW as well as its shape, micromagnetic simulations were performed. As described in the Supplemental Material S3 [47], we consider first both the anisotropy energy density that describes bulk materials as well as the magnetoelastic contributions to the effective field. In this case, it is possible to reproduce the Néel vector direction within the DW, however with larger magnetoelastic coupling coefficients. Besides, as described above, the considered anisotropy energy density must comply with the crystallographic conditions, which are incompatible with the observed domain structure. However, it is possible to fit the Néel vector direction within the DW by considering only the magnetoelastic interaction with different shear strains in the two domains. By disregarding the contribution of the anisotropy energy density, we are no longer assuming that the cubic cell is contracted along the ⟨111⟩ direction. Therefore, there is no reason to take the crystallographic restrictions as granted. In other words, we are implicitly assuming the cubic cell distortion is space modulated by the interface shear strain.

The micromagnetic simulations additionally provide the nanoscale DW profile that agrees with the experimental results, which are of course limited by the finite PEEM resolution. Therefore, a strip consisting of a T_1 domain with Néel vector direction along [$\bar{5}$ $\bar{5}$ 19] at one end and a T_3 domain with **n** along [$\bar{5}$ 5 19] at the other end was simulated. The dimension of the strip is 400×5 cells with a cell size of 0.5 nm, resulting in a total simulated volume of 200 nm $\times$ 2.5 nm with a thickness of 0.5 nm. The result of the simulation, including the DW in between the two domains, is shown in Fig. 4(a). Here, the black arrows visualize the in-plane rotation of the Néel vector and the color scheme visualizes the development of the n_z component of the Néel vector showing an increased out-of-plane component in the center of the DW, as observed experimentally. Figures 4(b)–4(d) show the extracted Néel vector components as a function of the position within the DW for the three spatial directions, where $x = [100]$, $y = [010]$, and $z = [001]$. The x and z components of the Néel vector along the DW can be approximated by a Gaussian function, while the y component can be represented by a distribution function. The width of the DWs in a magnetic thin film provides significant information about the material and its properties, since the DW width is determined by the ratio of anisotropy and exchange energy constant. However, it needs to be noted that the resolution of the PEEM microscope has an important influence on how wide certain structures appear in the XMLD-PEEM images and this needs to be taken into account when determining the DW width. Therefore, in order to be able to make a statement about the DW width, one must first determine the resolution limit of the microscope in the used configuration as shown in the Supplemental Material S4 [47]. For the determination of the DW width, the finite spatial resolution can be taken into account by fitting the signal convoluted with a Gaussian function with FWHM corresponding to the resolution limit [48]. For the fit the **E** vector is considered constant and given by the XMLD-PEEM image from which the data was extracted ($\gamma = 45°$, $\omega = 75°$) and **n** is defined by the DW profile. A linear function is added in order to depict the intensity gradient in the XMLD-PEEM image which can be observed in Fig. 4(f) as a linear decay. This yields a FWHM for the DWs between two 90° T domains of 98 ± 10 nm. We

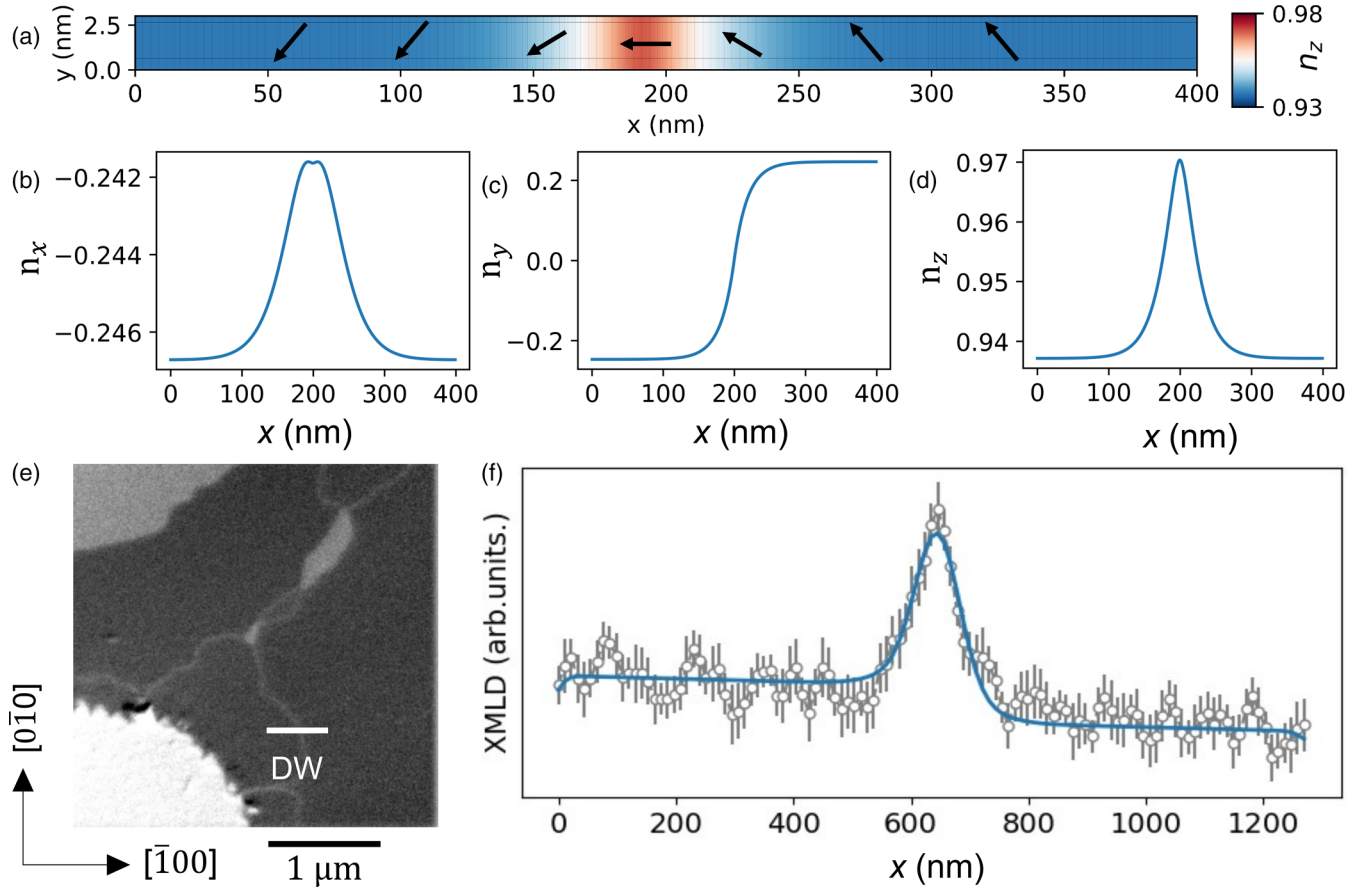

FIG. 4. (a) The simulation of a DW within a strip between a T_1 domain ([$\bar{5}$ $\bar{5}$ 19]) and a T_3 domain ([$\bar{5}$ 5 19]). Here the arrows indicate the in-plane rotation of the Néel vector and the color scheme visualizes the development of the n_z component of the Néel vector. The simulation allows one to read out the line profile of the Néel vector **n** change within a DW for (b) n_x, (c) n_y, and (d) n_z. The line profile extracted from the XMLD-PEEM image in (e) can be fitted by a convolution of the theoretical XMLD signal given by the simulation of the DW and the PEEM resolution limit (f).

would like to point out that this determined width is much larger than the resolution of the PEEM and is thus robust. In previous studies DWs with a width of 134–184 nm [34] up to several hundred nm [36] were observed in bulk NiO crystals. In comparison to these values the DWs observed in our thin films are narrow. This indicates that the anisotropy in our NiO thin films stemming from the substrate-induced strain is larger compared to the bulk, favoring in these thin films narrower DWs and in line with the observed change of the domain orientation from the {111} planes in the bulk to the [±5 ± 5 19] orientations found here. In terms of applications as storage devices, such narrow domain walls are favorable, since the DW width is a limit for the storage density.

III. CONCLUSION

By combining XMLD-PEEM imaging and current-induced switching we show that in insulating antiferromagnetic NiO/Pt thin films, arbitrary-shaped antiferromagnetic domain structures can be generated, indicating that the crystallographic restrictions present in bulk samples do not apply for thin films. We also show that the spins within the DW structure are always pointing in the same direction irrespective of their position in the path of the DW. This shows that the domain walls in our NiO(10 nm) sample are nonchiral, indicating the absence of strong Lifshitz invariants. Therefore, mechanisms predicting electrical switching of insulating antiferromagnetic films due to chirality-dependent movement of DWs [14,49] cannot explain the observed electrical switching of the magnetic structure. Further, we show that the Néel vector across the DW rotates on the shortest path between the Néel vector orientation of the two adjacent domains, thus increasing the anisotropy energy density. However, such increment in anisotropy energy is compensated by the reduction of the DW width and the exchange energy density. Using micromagnetic simulations we show that such a behavior of the Néel vector can be explained due to strain distribution within the NiO thin film. Extracting the simulated DW profile and fitting it to the XMLD data of the DW allows us to determine the width of the DW to $\Delta = 98 \pm 10$ nm. We note that to obtain the full profile of the domain wall, a higher resolution microscopy technique would be necessary, which however goes beyond the scope of this work. The observation of narrow DWs and their advantages for data storage devices underlines the importance of NiO in the context of AFM spintronics and the approach to make use of antiferromagnets as active elements in spintronic devices. For example, by varying the AFM film thickness, one could use the substrate-induced strain to tailor

the DW width to optimize the storage density in devices relying on antiferromagnetic materials and by this make use of the advantages AFMs possess over FMs.

ACKNOWLEDGMENTS

L.B. acknowledges the European Union's Horizon 2020 research and innovation program under the Marie Skłodowska-Curie Grant Agreement ARTES No. 793159. L.B., M.F., and M.K. acknowledge support from the Graduate School of Excellence Materials Science in Mainz (MAINZ) DFG 266, the DAAD (Spintronics network, Projects No. 57334897 and 57524834). We acknowledge that this work is funded by the Deutsche Forschungsgemeinschaft (DFG; German Research Foundation), TRR 173-268565370 (Spin+X Projects No. A01 and No. B02). This project has received funding from the European Union's Horizon 2020 research and innovation program under Grant Agreement No. 863155 (s-Nebula). We acknowledge Diamond Light Source for time on beamline I06 under Proposal No. MM22448. This work is also supported by ERATO "Spin Quantum Rectification Project" (Grant No. JPMJER1402) and the Grant-in-Aid for Scientific Research on Innovative Area, "Nano Spin Conversion Science" (Grant No. JP26103005), Grant-in-Aid for Scientific Research (S) (Grant No. JP19H05600), and Grant-in-Aid for Scientific Research (C) (Grant No. JP20K05297) from JSPS KAKENHI. R.R. also acknowledges support from the Grant RYC 2019-026915-I funded by the MCIN/AEI/10.13039/501100011033 and by the ESF investing in your future, the Xunta de Galicia (ED431F 2022/04, ED431B 2021/013, Centro Singular de Investigación de Galicia Accreditation 2019-2022, ED431G 2019/03) and the European Union (European Regional Development Fund - ERDF). L.S.T. and G.F. acknowledge financial support from the program "ASSEGNI DI RICERCA 2019" at the University of Messina, the project PRIN 2020LWPKH7 funded by the Italian Ministry of University and Research, and the PETASPIN association [53].

[1] V. Baltz, A. Manchon, M. Tsoi, T. Moriyama, T. Ono, and Y. Tserkovnyak, Antiferromagnetic spintronics, Rev. Mod. Phys. **90**, 015005 (2018).

[2] T. Kampfrath, A. Sell, G. Klatt, A. Pashkin, S. Mährlein, T. Dekorsy, M. Wolf, M. Fiebig, A. Leitenstorfer, and R. Huber, Coherent terahertz control of antiferromagnetic spin waves, Nat. Photonics **5**, 31 (2011).

[3] R. Lebrun, A. Ross, O. Gomonay, V. Baltz, U. Ebels, A.-L. Barra, A. Qaiumzadeh, A. Brataas, J. Sinova, and M. Kläui, Long-distance spin-transport across the Morin phase transition up to room temperature in ultra-low damping single crystals of the antiferromagnet α-Fe_2O_3, Nat. Commun. **11**, 6332 (2020).

[4] T. Moriyama, K. Oda, T. Ohkochi, M. Kimata, and T. Ono, Spin torque control of antiferromagnetic moments in NiO, Sci. Rep. **8**, 14167 (2018).

[5] X. Z. Chen, R. Zarzuela, J. Zhang, C. Song, X. F. Zhou, G. Y. Shi, F. Li, H. A. Zhou, W. J. Jiang, F. Pan, and Y. Tserkovnyak, Antidamping-Torque-Induced Switching in Biaxial Antiferromagnetic Insulators, Phys. Rev. Lett. **120**, 207204 (2018).

[6] L. Baldrati, O. Gomonay, A. Ross, M. Filianina, R. Lebrun, R. Ramos, C. Leveille, F. Fuhrmann, T. Forrest, F. Maccherozzi, S. Valencia, F. Kronast, E. Saitoh, J. Sinova, and M. Klaui, Mechanism of Néel Order Switching in Antiferromagnetic Thin Films Revealed by Magnetotransport and Direct Imaging, Phys. Rev. Lett. **123**, 177201 (2019).

[7] P. Zhang, J. Finley, T. Safi, and L. Liu, Quantitative Study on Current-Induced Effect in an Antiferromagnet Insulator/Pt Bilayer Film, Phys. Rev. Lett. **123**, 247206 (2019).

[8] H. Meer, F. Schreiber, C. Schmitt, R. Ramos, E. Saitoh, O. Gomonay, J. Sinova, L. Baldrati, and M. Kläui, Direct imaging of current-induced antiferromagnetic switching revealing a pure thermomagnetoelastic switching mechanism in NiO, Nano Lett. **21**, 114 (2021).

[9] E. Aytan, B. Debnath, F. Kargar, Y. Barlas, M. Lacerda, J. Li, R. Lake, J. Shi, and A. Balandin, Spin-phonon coupling in antiferromagnetic nickel oxide, Appl. Phys. Lett. **111**, 252402 (2017).

[10] L. Baldrati, C. Schmitt, O. Gomonay, R. Lebrun, R. Ramos, E. Saitoh, J. Sinova, and M. Kläui, Efficient Spin Torques in Antiferromagnetic CoO/Pt Quantified by Comparing Field- and Current-Induced Switching, Phys. Rev. Lett. **125**, 077201 (2020).

[11] A. Churikova, D. Bono, B. Neltner, A. Wittmann, L. Scipioni, A. Shepard, T. Newhouse-Illige, J. Greer, and G. Beach, Non-magnetic origin of spin Hall magnetoresistance-like signals in Pt films and epitaxial NiO/Pt bilayers, Appl. Phys. Lett. **116**, 022410 (2020).

[12] T. Shiino, S.-H. Oh, P. M. Haney, S.-W. Lee, G. Go, B.-G. Park, and K.-J. Lee, Antiferromagnetic Domain Wall Motion Driven by Spin-Orbit Torques, Phys. Rev. Lett. **117**, 087203 (2016).

[13] L. Sánchez-Tejerina, V. Puliafito, P. Khalili Amiri, M. Carpentieri, and G. Finocchio, Dynamics of domain-wall motion driven by spin-orbit torque in antiferromagnets, Phys. Rev. B **101**, 014433 (2020).

[14] L. Baldrati, A. Ross, T. Niizeki, C. Schneider, R. Ramos, J. Cramer, O. Gomonay, M. Filianina, T. Savchenko, D. Heinze *et al.*, Full angular dependence of the spin Hall and ordinary magnetoresistance in epitaxial antiferromagnetic NiO(001)/Pt thin films, Phys. Rev. B **98**, 024422 (2018).

[15] S. Arpaci, V. Lopez-Dominguez, J. Shi, L. Sánchez-Tejerina, F. Garesci, C. Wang, X. Yan, V. K. Sangwan, M. A. Grayson, M. C. Hersam *et al.*, Observation of current-induced switching in non-collinear antiferromagnetic $IrMn_3$ by differential voltage measurements, Nat. Commun. **12**, 3828 (2021).

[16] A. Hubert and R. Schäfer, *Magnetic Domains: The Analysis of Magnetic Microstructures* (Springer Science & Business Media, Berlin, Heidelberg, 2008).

[17] O. Shpyrko, E. Isaacs, J. Logan, Y. Feng, G. Aeppli, R. Jaramillo, H. Kim, T. Rosenbaum, P. Zschack, M. Sprung *et al.*, Direct measurement of antiferromagnetic domain fluctuations, Nature (London) **447**, 68 (2007).

[18] R. Jaramillo, T. F. Rosenbaum, E. D. Isaacs, O. G. Shpyrko, P. G. Evans, G. Aeppli, and Z. Cai, Microscopic and Macroscopic Signatures of Antiferromagnetic Domain Walls, Phys. Rev. Lett. **98**, 117206 (2007).

[19] M. Wörnle, P. Welter, Z. Kašpar, K. Olejník, V. Novák, R. Campion, P. Wadley, T. Jungwirth, C. Degen, and P. Gambardella, Current-induced fragmentation of antiferromagnetic domains, arXiv:1912.05287.

[20] F. Radu and H. Zabel, Exchange bias effect of ferro-/antiferromagnetic heterostructures, Springer Tracts Mod. Phys. **227**, 97 (2008).

[21] M. S. Wörnle, P. Welter, M. Giraldo, T. Lottermoser, M. Fiebig, P. Gambardella, and C. L. Degen, Coexistence of Bloch and Néel walls in a collinear antiferromagnet, Phys. Rev. B **103**, 094426 (2021).

[22] K. M. D. Hals, Y. Tserkovnyak, and A. Brataas, Phenomenology of Current-Induced Dynamics in Antiferromagnets, Phys. Rev. Lett. **106**, 107206 (2011).

[23] O. Gomonay, T. Jungwirth, and J. Sinova, High Antiferromagnetic Domain Wall Velocity Induced by Néel Spin-Orbit Torques, Phys. Rev. Lett. **117**, 017202 (2016).

[24] D. Bossini, M. Pancaldi, L. Soumah, M. Basini, F. Mertens, M. Cinchetti, T. Satoh, O. Gomonay, and S. Bonetti, Ultrafast Amplification and Nonlinear Magnetoelastic Coupling of Coherent Magnon Modes in an Antiferromagnet, Phys. Rev. Lett. **127**, 077202 (2021).

[25] O. Gomonay and D. Bossini, Linear and nonlinear spin dynamics in multi-domain magnetoelastic antiferromagnets, J. Phys. D **54**, 374004 (2021).

[26] M. J. Grzybowski, P. Wadley, K. W. Edmonds, R. Beardsley, V. Hills, R. P. Campion, B. L. Gallagher, J. S. Chauhan, V. Novak, T. Jungwirth, F. Maccherozzi, and S. S. Dhesi, Imaging Current-Induced Switching of Antiferromagnetic Domains in CuMnAs, Phys. Rev. Lett. **118**, 057701 (2017).

[27] A. A. Sapozhnik, M. Filianina, S. Y. Bodnar, A. Lamirand, M.-A. Mawass, Y. Skourski, H.-J. Elmers, H. Zabel, M. Kläui, and M. Jourdan, Direct imaging of antiferromagnetic domains in Mn_2Au manipulated by high magnetic fields, Phys. Rev. B **97**, 134429 (2018).

[28] J. Xu, C. Zhou, M. Jia, D. Shi, C. Liu, H. Chen, G. Chen, G. Zhang, Y. Liang, J. Li *et al.*, Imaging antiferromagnetic domains in nickel oxide thin films by optical birefringence effect, Phys. Rev. B **100**, 134413 (2019).

[29] J. Xu, H. Chen, C. Zhou, D. Shi, G. Chen, and Y. Wu, Optical imaging of antiferromagnetic domains in ultrathin CoO(001) films, New J. Phys. **22**, 083033 (2020).

[30] F. Schreiber, L. Baldrati, C. Schmitt, R. Ramos, E. Saitoh, R. Lebrun, and M. Kläui, Concurrent magneto-optical imaging and magneto-transport readout of electrical switching of insulating antiferromagnetic thin films, Appl. Phys. Lett. **117**, 082401 (2020).

[31] S.-W. Cheong, M. Fiebig, W. Wu, L. Chapon, and V. Kiryukhin, Seeing is believing: Visualization of antiferromagnetic domains, npj Quantum Mater. **5**, 1 (2020).

[32] S.-H. Yang, K.-S. Ryu, and S. Parkin, Domain-wall velocities of up to 750 m s^{-1} driven by exchange-coupling torque in synthetic antiferromagnets, Nat. Nanotechnol. **10**, 221 (2015).

[33] M. Bode, E. Vedmedenko, K. Von Bergmann, A. Kubetzka, P. Ferriani, S. Heinze, and R. Wiesendanger, Atomic spin structure of antiferromagnetic domain walls, Nat. Mater. **5**, 477 (2006).

[34] N. B. Weber, H. Ohldag, H. Gomonaj, and F. U. Hillebrecht, Magnetostrictive Domain Walls in Antiferromagnetic NiO, Phys. Rev. Lett. **91**, 237205 (2003).

[35] G. A. Slack, Crystallography and domain walls in antiferromagnetic NiO crystals, J. Appl. Phys. **31**, 1571 (1960).

[36] K. Arai, T. Okuda, A. Tanaka, M. Kotsugi, K. Fukumoto, T. Ohkochi, T. Nakamura, T. Matsushita, T. Muro, M. Oura *et al.*, Three-dimensional spin orientation in antiferromagnetic domain walls of NiO studied by x-ray magnetic linear dichroism photoemission electron microscopy, Phys. Rev. B **85**, 104418 (2012).

[37] F. Krizek, S. Reimers, Z. Kašpar, A. Marmodoro, J. Michalička, O. Man, A. Edström, O. J. Amin, K. W. Edmonds, R. P. Campion *et al.*, Atomically sharp domain walls in an antiferromagnet, Sci. Adv. **8**, eabn3535 (2022).

[38] M. R. K. Akanda, I. J. Park, and R. K. Lake, Interfacial Dzyaloshinskii-Moriya interaction of antiferromagnetic materials, Phys. Rev. B **102**, 224414 (2020).

[39] G. R. Hoogeboom, A. Aqeel, T. Kuschel, T. T. Palstra, and B. J. van Wees, Negative spin Hall magnetoresistance of Pt on the bulk easy-plane antiferromagnet NiO, Appl. Phys. Lett. **111**, 052409 (2017).

[40] J. Fischer, O. Gomonay, R. Schlitz, K. Ganzhorn, N. Vlietstra, M. Althammer, H. Huebl, M. Opel, R. Gross, S. T. B. Goennenwein, and S. Geprags, Spin Hall magnetoresistance in antiferromagnet/heavy-metal heterostructures, Phys. Rev. B **97**, 014417 (2018).

[41] T. Moriyama, K. Hayashi, K. Yamada, M. Shima, Y. Ohya, and T. Ono, Tailoring THz antiferromagnetic resonance of NiO by cation substitution, Phys. Rev. Mater. **4**, 074402 (2020).

[42] W. L. Roth, Neutron and optical studies of domains in NiO, J. Appl. Phys. **31**, 2000 (1960).

[43] T. Nussle, P. Thibaudeau, and S. Nicolis, Coupling magnetoelastic Lagrangians to spin transfer torque sources, J. Magn. Magn. Mater. **469**, 633 (2019).

[44] W. L. Roth and G. A. Slack, Antiferromagnetic structure and domains in single crystal NiO, J. Appl. Phys. **31**, S352 (1960).

[45] C. Schmitt, L. Baldrati, L. Sanchez-Tejerina, F. Schreiber, A. Ross, M. Filianina, S. Ding, F. Fuhrmann, R. Ramos, F. Maccherozzi, D. Backes, M. A. Mawass, F. Kronast, S. Valencia, E. Saitoh, G. Finocchio, and M. Kläui, Identification of Néel Vector Orientation in Antiferromagnetic Domains Switched by Currents in NiO/Pt Thin Films, Phys. Rev. Appl. **15**, 034047 (2021).

[46] H. Meer, O. Gomonay, C. Schmitt, R. Ramos, L. Schnitzspan, F. Kronast, M.-A. Mawass, S. Valencia, E. Saitoh, J. Sinova *et al.*, Strain-induced shape anisotropy in antiferromagnetic structures, Phys. Rev. B **106**, 094430 (2022).

[47] See Supplemental Material at http://link.aps.org/supplemental/10.1103/PhysRevB.107.184417 for a comparison of the domain walls in the center of the Hall cross and at the edge; details on the determination of Néel vector orientation within the domain wall; details on the micromagnetic simulations; and details on the determination of the resolution of the PEEM images. The Supplemental Material also contains Refs. [13,45,48,50–52].

[48] O. Boulle, J. Vogel, H. Yang, S. Pizzini, D. de Souza Chaves, A. Locatelli, T. O. Menteş, A. Sala, L. D. Buda-Prejbeanu, O. Klein *et al.*, Room-temperature chiral magnetic skyrmions in

ultrathin magnetic nanostructures, Nat. Nanotechnol. **11**, 449 (2016).

[49] I. Gray, T. Moriyama, N. Sivadas, G. M. Stiehl, J. T. Heron, R. Need, B. J. Kirby, D. H. Low, K. C. Nowack, D. G. Schlom, D. C. Ralph, T. Ono, and G. D. Fuchs, Spin Seebeck Imaging of Spin-Torque Switching in Antiferromagnetic Pt/NiO Heterostructures, Phys. Rev. X **9**, 041016 (2019).

[50] H. V. Gomonay and V. M. Loktev, Spin transfer and current-induced switching in antiferromagnets, Phys. Rev. B **81**, 144427 (2010).

[51] V. Puliafito, R. Khymyn, M. Carpentieri, B. Azzerboni, V. Tiberkevich, A. Slavin, and G. Finocchio, Micromagnetic modeling of terahertz oscillations in an antiferromagnetic material driven by the spin Hall effect, Phys. Rev. B **99**, 024405 (2019).

[52] P. Popov, A. Safin, A. Kirilyuk, S. Nikitov, I. Lisenkov, V. Tyberkevich, and A. Slavin, Voltage-Controlled Anisotropy and Current-Induced Magnetization Dynamics in Antiferromagnetic-Piezoelectric Layered Heterostructures, Phys. Rev. Appl. **13**, 044080 (2020).

[53] See https://www.petaspin.com.